Fe–Cr–Ni–Co–Cu_x coatings for marine and coastal infrastructure protection from corrosion, tribocorrosion and biofouling

M. N. Fatykhova, *Junior Researcher*[1]*, e-mail: mariya.antonyuck@ya.ru;*
A. N. Sheveyko, *Researcher*[1]*, e-mail: sheveyko@mail.ru;*
A. R. Gizatullina*, Research Assistant*[1]*, e-mail: alfina.gizatullina@yandex.ru;*
K. A. Kuptsov, *Senior Researcher*[1]*, e-mail: kuptsov.k@gmail.com*

[1] *National University of Science and Technology "MISIS" (Moscow, Russia)*

The aim of this study is to investigate the effect of varying copper (Cu) content on the structure, corrosion, tribocorrosion, and bactericidal properties of FeCrNiCo–Cu_x coatings. Specifically, the main idea is to maximize the Cu content without secondary phases formation using Electrospark Deposition (ESD) method characterized by rapid cooling rates of the melt, while maintaining the corrosion properties of the Cu-free coating, and simultaneously enhancing its antimicrobial and tribocorrosion properties. To achieve this, thick high-entropy Fe–Cr–Ni–Co–(Cu) coatings with different Cu content (up to 24 at. %) were obtained in a protective argon atmosphere. All coatings exhibited a single-phase structure based on a solid solution with an fcc lattice, dense and homogeneous microstructure with high continuity. In tribocorrosion conditions, the FeCrNiCo coating demonstrated the lowest corrosion current, while the FeCrNiCo–12Cu coating revealed the most positive corrosion potential. However, after a certain Cu content threshold, tribocorrosion behavior deteriorated significantly. In terms of wear, coatings with high Cu content exhibited the highest wear resistance, which did not correlate with the hardness of the coatings. All coatings demonstrated a moderate antibacterial effect against B. cereus Arc30, with the FeCrNiCo–12Cu coating showing the highest ability to suppress bacterial growth and further biofilm formation.

Key words: Coatings, HEA, HECs, tribocorrosion, corrosion, antibacterial, seawater.
DOI: 10.17580/cisisr.2025.01.16

Introduction

In marine and coastal infrastructure, a great variety of metal materials such as carbon steel, stainless steel, aluminum-, copper-, and titanium-based alloys are commonly used for their specific properties and advantages [1–4]. However, carbon steel is still a material of choice in many applications due to its high strength, cost-effectiveness, and ease of welding [2].

Seawater, an aqueous solution of salts and suspended particles, is characterized by high salinity, chlorinity, and a dissolved oxygen content that varies with temperature and depth. It also contains heavy metals and dissolved gases like CO_2, NH_3, and H_2S, introduced through effluents discharge, which can decompose into toxic, corrosive components [5, 6].

Corrosion of marine infrastructure is influenced by a variety of factors, including non-biological (corrosive ions, wind, waves, and light) and biological (fouling organisms and microorganisms) factors. Recent research has demonstrated that fouling organisms significantly impact marine facilities, with biofouling emerging as a global challenge that limits the development of marine resources [7].

Metallic materials used in marine and coastal infrastructure encounter several significant challenges. These challenges primarily include corrosion and tribocorrosion (term used to determine combined synergetic processes of wear and corrosion), fatigue, strength losses, brittle fracture, and cracking [2, 8].

Microbiologically-influenced corrosion (MIC) is also a significant issue in marine infrastructure resulting in accelerated corrosion of metallic surfaces [9–11]. Various bacteria and microorganisms participate in MIC in marine environment including Sulfate-Reducing Bacteria (SRB), Iron-Oxidizing Bacteria (IOB), Sulfur-Oxidizing Bacteria (SOB), and Manganese-Oxidizing Bacteria (MOB). Initially, a clean metal surface is exposed to microorganisms in a marine environment. These microorganisms attach to the surface, forming a biofilm that facilitates microbial adhesion and metabolic activities, resulting in corrosive byproducts (for example, H_2S formation by SRB), changed pH of the local environment and localized corrosion. As the biofilm matures, it attracts additional organisms, leading to macrobiofouling. Preventing and suppressing biofouling and MIC in marine environment involves surface modification, organic inhibitors and biocide treatment, and cathodic protection [12].

To address these challenges, various strategies are utilized with a primary focus on corrosion resistance without altering their volume or structure [13]. These include the use of corrosion-resistant materials like stainless steel and alloys

[14,15], cathodic protection via sacrificial anodes or current systems [16], surface treatments and coatings [17, 18] like marine-grade paints [19], epoxy [20], or metallic/ceramic/composite coatings [21, 22], and inhibitors that form protective layers or react with corrosive agents [23].

Copper (Cu) is known to suppress MIC and biofouling due to its antimicrobial properties [24–29]. Studies have shown that Cu ions disrupt microbial cell membranes, enzymes, and DNA, leading to reduced microbial viability and ability to colonize metal surfaces [15, 29]. Moreover, the formation of Cu complexes with extracellular polymeric substances in biofilms can disrupt their integrity.

For example, Cu–Ti coatings demonstrated effective and long-term antifouling performance by enabling controlled release of Cu ions from Cu–Ti micro-galvanic cells [27]. Also, composite Cu–Cu_2O coatings deposited on submarine screen doors released Cu ions via electrochemical dissolution, forming a copper-rich water film that deterred biofouling [24]. Cu-modified pipeline steel and Cu-bearing bainite type grade R5 mooring chain steels have shown improved resistance to MIC [30, 31]. Additionally, the Cu-alloyed AISI 8630 and duplex 2205-Cu-DSS steels showed a reduction of pit depth and inhibition of biofilm growth due to the formation of protective Cu_2O and CuO layers [32, 33].

Coatings based on high-entropy coatings (HECs) have demonstrated excellent properties such as high strength [34], toughness [35], temperature oxidation resistance [36], corrosion resistance [37], wear resistance [38], unique electrical and magnetic properties [39], and biocompatibility [40]. Main reason behind the novel behavior of HECs is the four different core mechanisms/effects: (1) high entropy effects, (2) severe lattice distortion, (3) sluggish diffusion, and (4) cocktail effects [41].

HEA systems, which contain one or more passivating elements (Cr, Ni, Mo, etc.) revealed equivalent or superior corrosion-resistant properties compared with conventional alloys [42]. Economically, cost of HEAs production can be high due to the expensive alloying elements, while coatings offer a cost-effective solution to this issue. Moreover, it is reported that coatings based on high-entropy alloys (HECs) with the same composition as the bulk material demonstrate even better corrosion-resistant properties [42].

A range of high-entropy coatings (HECs) demonstrating enhanced corrosion resistance in chlorine-containing media, such as (Al)FeCoNiCr [43], FeCoNiCrCu [44], CoCrFeNiTi–(Mo) [42], Al(Cr)NiCoFeCu [45] and $FeCoNiCuSn_x$ [46] have been recently developed. Popular methods for HECs deposition include laser cladding, electro-spark deposition, chemical-vapor deposition, and magnetron sputtering [42]. Main approach here is the alloying of base FeCrNiCo material with additional elements such as Al, Ti, Mo, Cu etc. and playing with portion of Fe, Cr, Ni and Co in the base coatings. However, in most cases base non-alloyed FeCrNiCo HECs demonstrated superior corrosion characteristics.

Introduction of Cu into FeCrNiCo may lead to formation of two-phase fcc/bcc structure [45] or Cu segregation in interdendrites leading to Cu-rich and Cu-depleted zones formation [46]. Due to the weaker binding force with other elements such as Fe, Co, Ni, and Cr, copper tends to segregate as Cu-rich clusters, which leads to intensified localized corrosion. However, recent investigations demonstrated that in FeCrNiCo–Cu coatings with 13 at. % Cu obtained by electrospark deposition in vacuum no secondary phases formation was observed due to rapid solidification typical for ESD [47]. Also, studies on Fe–Cr–Ni–Co–(Cu) HECs revealed their superior tribocorrosion resistance in marine environment [47–49].

The aim of this study is to investigate the effect of varying copper (Cu) content on the structure, corrosion, tribocorrosion, and bactericidal properties of FeCrNiCo-Cu_x coatings. Specifically, we aim to maximize the Cu content without secondary phases formation using Electrospark Deposition method, while maintaining the corrosion properties of the Cu-free coating, and simultaneously enhancing its antimicrobial and tribocorrosion properties.

2. Experimental part

2.1. Electrodes

For the high-entropy FeCrNiCo–Cu_x coatings deposition, Fe–Co–Cr–Ni–Cu_x electrodes (x = 0, 10, 15, and 30 at. %) with varying copper content were produced using powder metallurgy methods described elsewhere [50]. Metallic powders of iron (VK-3, 9 μm), nickel (PNK-UT3, 10 μm), cobalt (PK-1u, 45-71 μm), chromium (PM-ERKh, 80 μm), and copper (PMS-1, 50–70 μm) were used as precursors.

The power mixture for the electrodes was obtained by high-energy mechanical alloying using a planetary centrifugal mill (PCM) "Activator-2s" (OOO "Zavod Khimicheskogo Mashinistroeniya", Russia). Rotation speed of the drums was 694 rpm, mill operating time was 30 min, and mass ratio of grinding bodies (steel balls) and the powder was 15:1. The mill drums were filled with Ar to avoid powder oxidation.

The electrodes were produced from the prepared mixture by direct hot pressing using a DSP-515 SA press (Dr. Fritsch, Germany) at a temperature of 950 °C, pressure of 35 MPa and an isobaric holding for 3 min.

2.2. Coatings deposition

High-entropy Fe–Co–Cr–Ni–Cu_x coatings were obtained by electrospark deposition (ESD) using an "Alier-303 metal" setup in manual mode in an Ar environment under following regimes: pulse frequency 1600 Hz, pulse current 120 A and pulse duration 40 μs. Discs with a diameter of 30 mm made of 30Kh13 steel were used as a substrate. The deposition time of each coating was 25 min. The coatings labelled Cu0 (without copper), Cu1, Cu2, Cu3 were obtained using Fe–Co–Cr–Ni, Fe–Co–Cr–Ni–Cu_{10}, Fe–Co–Cr–Ni–Cu_{15}, FeCo–Cr–Ni–Cu_{30}, electrodes, respectively.

2.3. Structure and elemental composition

The structure, elemental and phase composition of the electrodes and coatings were investigated by scanning electron microscopy (SEM) on an S-3400N microscope (Hitachi) equipped with a NORAN energy dispersive detector (EDS) and X-ray diffraction analysis (XRD) using

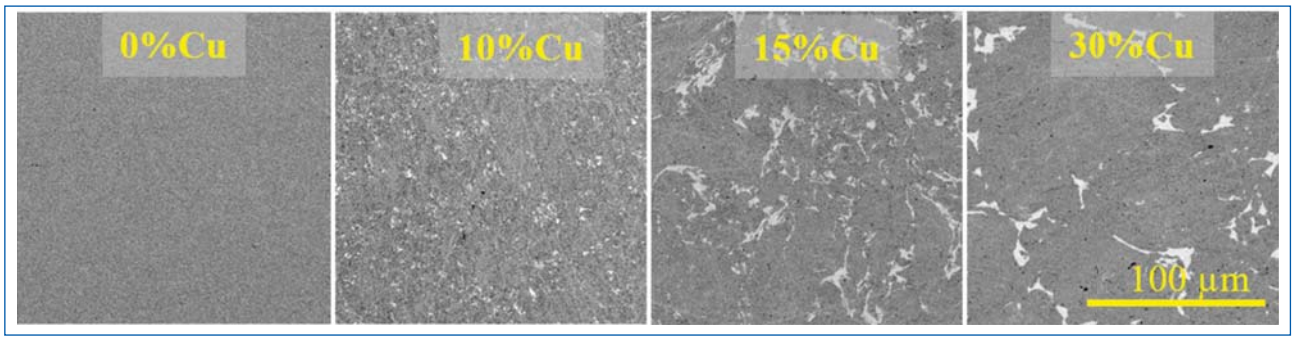

Fig. 1. Cross-section SEM images of Fe–Co–Cr–Ni–Cu_x electrodes (x = 0, 10, 15, 30 at. %)

a D8 Advance diffractometer (Bruker). Electrodes structure was studied on cross-sections prepared by polishing using abrasive paper from 320 to 1200 followed by finish polishing with OP-S suspension.

2.4. Coatings' properties investigations

Hardness of the coatings was measured by a microindentation method using a DuraScan 70 microhardness tester (EMCO-TEST Prüfmaschinen GmbH, Austria) at a load of 0.5 N. For each coating, ten individual measurements were carried out and average hardness values were calculated.

All corrosion and tribocorrosion studies were performed in artificial seawater prepared in accordance with ASTM D 1141-98 (paragraph 6, solution without heavy metal ions). Tribocorrosion behavior was studied using a tribometer (CSM Instruments) operating in a "ball-on-disc" under the following conditions: Al_2O_3 ball counterbody (6 mm in diameter), load 5 N, sliding speed 10 cm/s, distance 500 m. Surface roughness and wear tracks profiles of the coatings were investigated using optical profilometer Wyko-NT1100 (Veeco, USA). The tribometer was equipped with a rotating three-electrode cell to carry out electrochemical experiments both under steady-state conditions and during tribological tests. The cell was equipped with an Ag/AgCl reference electrode and an auxiliary Pt electrode. Potential and corrosion currents were measured using a VoltaLab 50 potentiostat (Radiometer Analytical). Potentiodynamic measurements were carried out at polarization ranging from –200 to +500 mV with respect to open circuit potential (OCP) at a 1 mV/s scan rate. All potentials were recalculated to a standard hydrogen electrode (SHE). Corrosion currents were calculated using the Tafel extrapolation method.

Antibacterial activity of the coatings was assessed against B. cereus Arc30 bacteria. All samples were sterilized using UV radiation for 60 min before experiments. Each sample was placed in a well with 4 ml of saline solution, and two more wells without samples were used as a control. Simultaneously, 0.05 ml of a suspension containing 3h-broth culture of the test strain with a concentration of 10^9 CFU/ml in saline solution was added to all wells. Incubation was carried out at 37 °C. After 0, 6 and 24 h of incubation, 0.04 ml was taken from each well to determine the CFU concentration.

The CFU concentration was determined by decimal dilutions in 0.3 ml of saline. From each dilution, 0.01 ml of bacterial suspension was transferred to Petri dishes with Mueller Hinton Agar nutrient medium (HiMedia, India), dried in a closed cup at room temperature for 10 min, and then cultured at 37 °C for 24 h.

3. Results and discussion

3.1. Electrodes

Fig. 1 shows SEM images of Fe–Co–Cr–Ni–Cu_x (x = 0, 10, 15, 30 at. %) electrode crosssections. All electrodes exhibit high continuity (residual porosity less than 1 %). The Fe–Co–Cr–Ni electrode without copper was characterized by a homogeneous morphology, while introduction of copper in electrodes led to bright Cu-rich clusters formation. As the copper content in the electrodes increased, the clusters became larger, however, their total number decreased.

3.2. Mass transfer kinetics

Fig. 2 demonstrates the results of the mass transfer kinetics studies for Cu0 and Cu3 coatings deposited with Cu-free (FeCrNiCo) and Cu-maximum (FeCrNiCo–Cu_{30}) electrodes, respectively, as a function of the processing time. In case of both electrodes, a monotonous increase in the mass of the coatings and erosion of the electrodes are observed when the processing time is increased from 3 to 12 min. However, Cu-maximum electrode demonstrated two times more efficient mass transfer starting from 3 min of processing, which is probably due to the presence of low-melting copper in the electrodes.

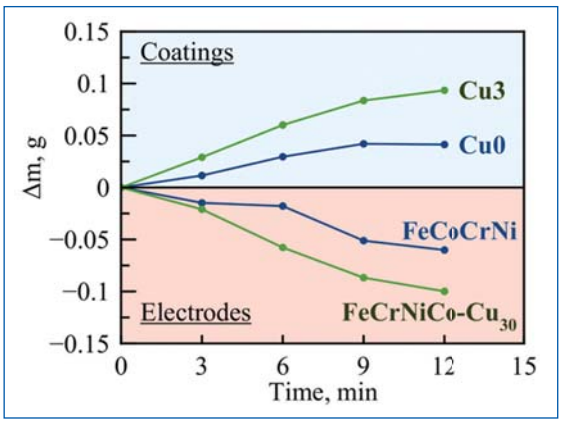

Fig. 2. Change in mass of Fe–Cr–Ni–Co and Fe–Cr–Ni–Co–Cu_{30} electrodes and corresponding Cu0 and Cu3 coatings as a function of processing time

3.3. Composition and microstructure of coatings

Fig. 3 displays SEM images of the surface of Fe–Cr–Ni–Co–Cu_x coatings and corresponding elemental distribution EDS maps. Coatings Cu0, Cu1 and Cu2 demonstrate homogeneous, crack-free morphology. Coating with the maximum copper content (Cu3) reveals the local defects in the form of cracks. The roughness of the coatings (R_a) is similar and falls in the range of 3.2–3.5 μm.

Fig. 4 shows the cross-sectional SEM images of the coatings, as well as corresponding Cu and Fe maps and distribution profiles. All coatings, including Cu3, demonstrate continuous and defect-free structure. In Cu1–Cu3 coatings, copper is distributed uniformly (Fig. 3*b*). With increase in Cu content, increase in the coatings thickness is observed from 14 (Cu0) to 23 μm (Cu3) caused by the intensification of mass transfer when using Cu-containing electrodes (Fig. 2). In Cu0 and Cu1 coatings, a monotonous increase in Fe content in the direction from surface to substrate from 39 to 87 at. %, respectively, was observed. In Cu2 and Cu3 coatings, two areas can be distinguished: the main coating layer up to 17 μm thick, characterized by a relatively uniform distribution of elements, and the transition layer between the coating and the substrate with a smooth increase in Fe and a decrease in Co, Ni and Cu concentrations (**Table 1**). The thickness of the transition layer in Cu3 coating is significantly greater than that of Cu2 coating (13 and 7 μm, respectively).

The EDS elemental composition of the coatings was determined both on the surface and on the cross-sections and the average values are presented in Table 1. The Cu content in the coatings increases proportionally with the increase in Cu content in the electrodes being 8 (Cu1), 12 (Cu2) and 25 at. % (Cu3), respectively. With increase in Cu content, the concentration of Fe monotonically decreases from 59 (Cu0) to 34 at. % (Cu3), while the content of other metallic elements remains almost constant. All coatings are characterized by high Cr (17–20 at. %) and moderate Co and Ni (11–14 at. %) content.

All coatings are characterized by a single-phase solid solution structure with FCC lattice (**Fig. 5**). No secondary copper-based phases were detected. The lattice parameter increases from 3.557 (Cu0) to 3.583 Å (Cu3) with increasing Cu content in the coatings due to higher incorporation

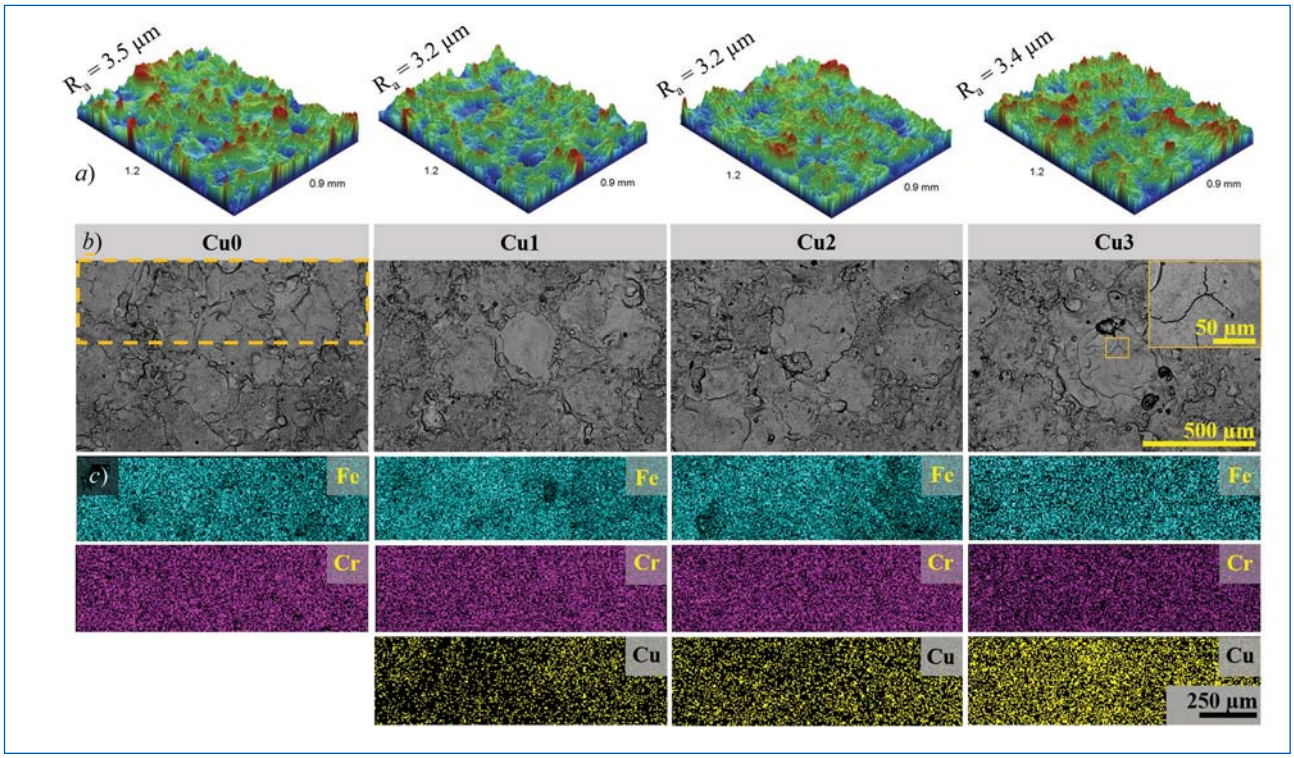

Fig. 3. 3D profiles (*a*) and SEM images of the surface of Fe–Cr–Ni–Co–Cu_x coatings (*b*), as well as the corresponding element distribution maps (*c*)

Table 1. Elemental composition and typical thicknesses of Fe–Cr–Ni–Co–Cu_x coatings

Coatings	Thickness, μm	Transition layer thickness, μm	Cr	Fe	Co	Ni	Cu
			at. %				
Cu0	14	< 1	20	56	12	12	–
Cu1	20	< 1	19	48	12	13	8
Cu2	24	7	19	42	13	14	12
Cu3	29	13	17	34	11	13	25

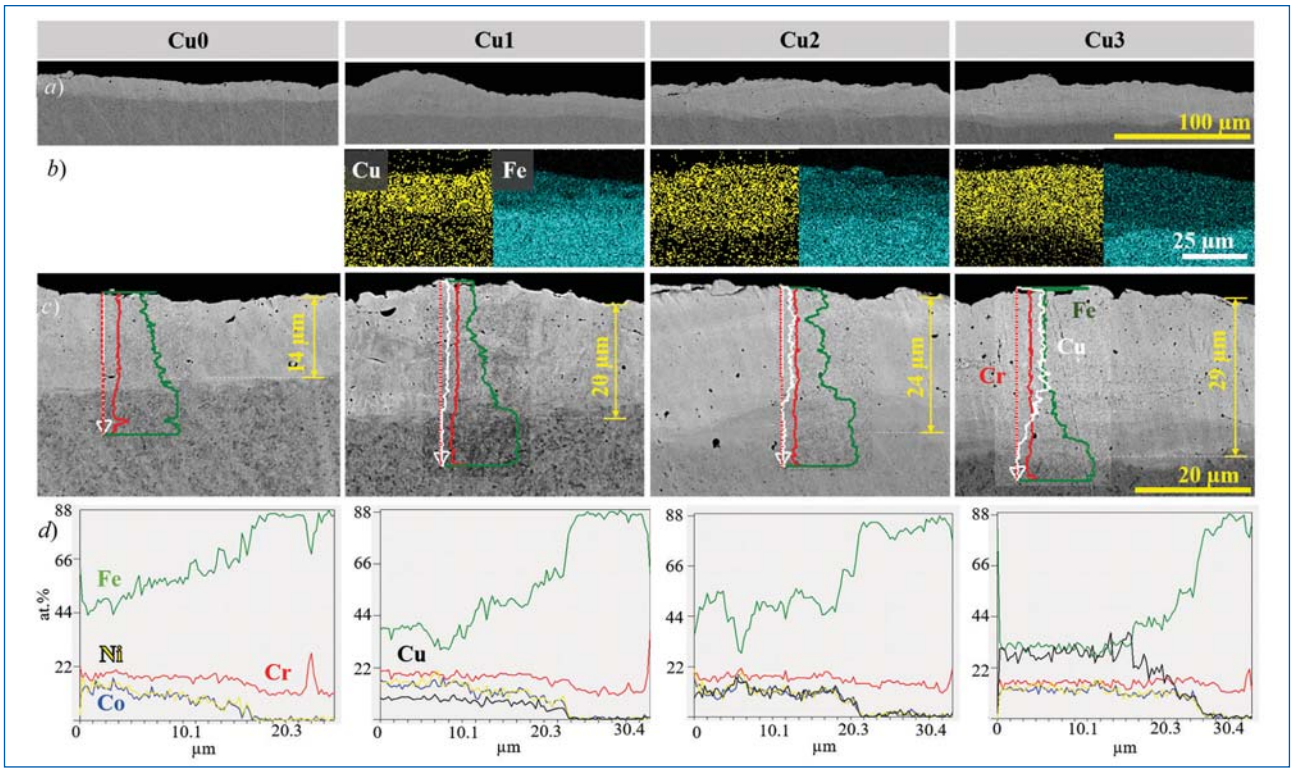

Fig. 4. Cross-sectional SEM images of Fe–Cr–Ni–Co–Cu_x coatings at different magnifications (*a*, *c*), EDS maps of Cu and Fe distribution in the coatings (*b*) and profiles of element distribution over the thickness of coatings (*d*)

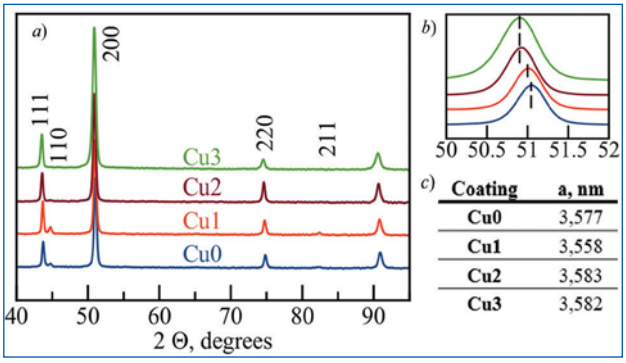

Fig. 5. XRD patterns of Fe–Cr–Ni–Co–Cu_x coatings (*a*, *b*) and corresponding lattice parameters (*c*)

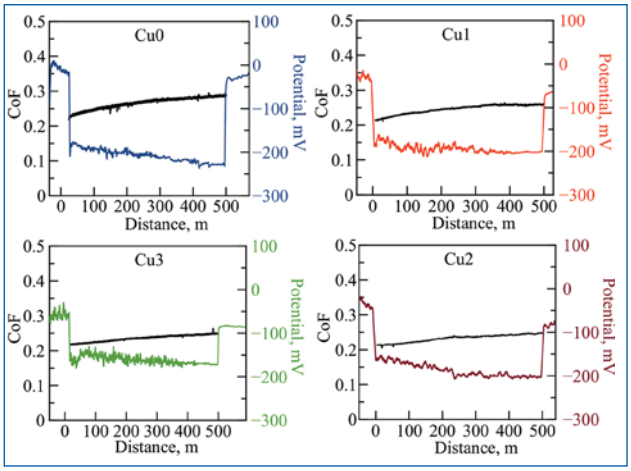

Fig. 6. Coefficient of friction and corrosion potential values of Fe–Cr–Ni–Co–Cu_x coatings measured during tribocorrosion tests in artificial seawater

of Cu into the fcc phase (Fig. 5 *b*, *c*). Low intensity peaks at 44.5° and 82° correspond to α-Fe from substrate.

3.4. Tribocorrosion and electrochemical behavior

Fig. 6 exhibits the dependencies of the coefficient of friction (CoF) and corrosion potential (CP) of the coatings on the sliding distance. At the first stage of tribocorrosion studies, the coatings were kept under stationary conditions to stabilize the corrosion potentials. It is revealed that increase in Cu content is associated with a decrease in the open circuit potentials from +0 (Cu0) to –53 mV (Cu3). This effect is probably due to the formation of a higher amount of loose CuO in the passive film, which deteriorates its properties [51].

Under friction, all coatings showed a sharp drop in CP due to the removal of the passive film. After the sharp drop, there was a slight monotonic decrease in CP until the end of the experiment. For the Cu-free coating, the CP decreased from –180 to –225 mV. Cu1 and Cu2 coatings exhibited higher CP values from –160 mV (beginning) to –200 mV (end). The coating with maximum Cu content possessed the minimum CP drop during friction (from –150 to –160 mV), demonstrating better corrosion resistance during wear.

After friction was stopped, an immediate increase in CP was observed, indicating passive film recovery in the wear tracks. In Cu0 coating, the CP increased to the initial value of –20 mV, while Cu-containing coatings only partial CP recovery to –60, –80 and -90 mV (Cu1, Cu2, Cu3) was

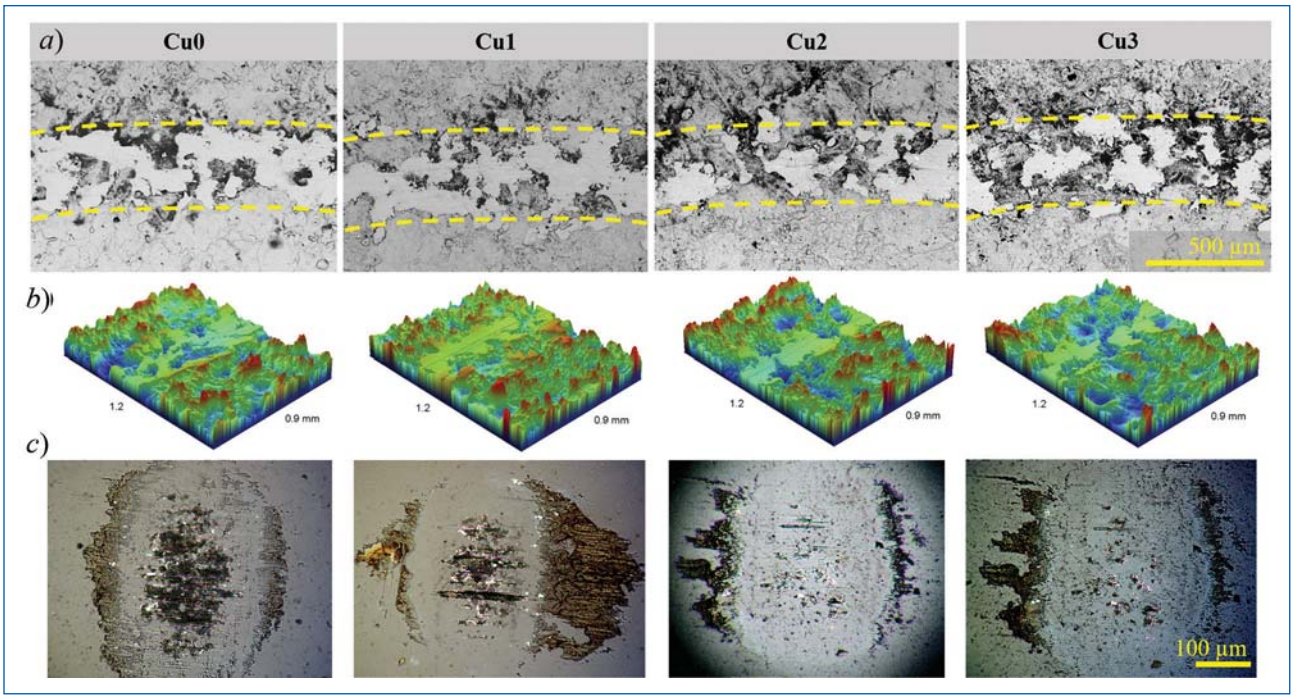

Fig. 7. SEM images of wear tracks of Fe–Cr–Ni–Co–Cux coatings (*a*) and their corresponding 3D profiles (*b*), as well as optical images of the counter-body (Al_2O_3 ball) after tribocorrosion studies (*c*)

observed. This effect is probably due to the dirrefern composition of recovered passive film compared to that of the initial surface.

The CoF values of the coatings during tribocorrosion experiments differed insignificantly and monotonically increased with increasing distance from 0.20 to 0.26.

Fig. 7 compares SEM images of the wear tracks of FeCrNiCo–Cu_x coatings. All wear tracks have a similar morphology representing partial wear of the surface roughness (Fig. 7*a*, *b*). The areas between the worn areas are filled with wear and corrosion products consisting mainly of Fe and Cr oxides and artificial seawater components.

Fig. 7*c* shows optical images of the counterbody (Al_2O_3 ball) after tribocorrosion studies. All balls show traces of wear products. The ball surface after friction of Cu0 coating was characterized by severe wear. With the increase in Cu content in the coatings, a decrease in the wear spot on the counterbody was observed, probably due to the increase in content of soft copper oxide in the wear debris.

For reliable assessment of the wear rate, the surface of the coatings was polished to roughness R_a = 0.2 μm and tribological tests were repeated.

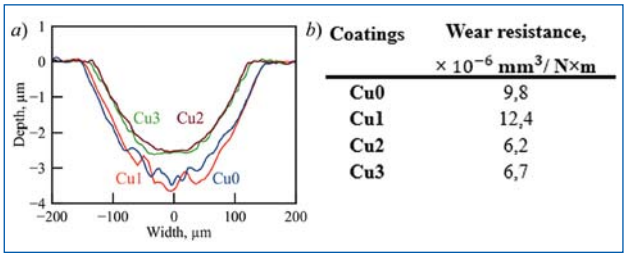

Fig. 8. 2D profiles of wear tracks of Fe–Cr–Ni–Co–Cu_x coatings (*a*) and their corresponding wear rate values (*b*)

The wear track profiles of Fe–Cr–Ni–Co–Cu_x coatings with the corresponding wear rate values are combined in **Fig. 8**. All coatings reveal enhanced wear resistance, however, the Cu2 and Cu3 coatings were the most wear resistant demonstrating wear rates of 6.2×10^{-6} and 6.7×10^{-6} mm³/Nm, respectively. Cu0 and Cu1 coatings showed more significant wear in tribocorrosion tests ($9.8–12.4\times10^{-6}$ mm³/N×m).

Interestingly, the wear resistance of the coatings does not show a correlation with their hardness. As the Cu content increases, the hardness of the coatings consistently decreases from 3.3 (Cu0) to 2.9 GPa (Cu3), as depicted in **Fig. 9*a*.** In addition, all coatings are characterized by a high crack resistance. In microindentation tests, neither radial nor ring cracks are observed in the indentation region (Fig. 9*b*).

The polarization curves of the coatings, derived from electrochemical tests in artificial seawater, are illustrated in **Fig. 10**. With the increase in Cu content from 0 (Cu0) to 12 (Cu2) at. %, a shift of the corrosion potential in the positive direction from +44 to + 130 mV occurs, which is accompanied by an increase in corrosion current density from

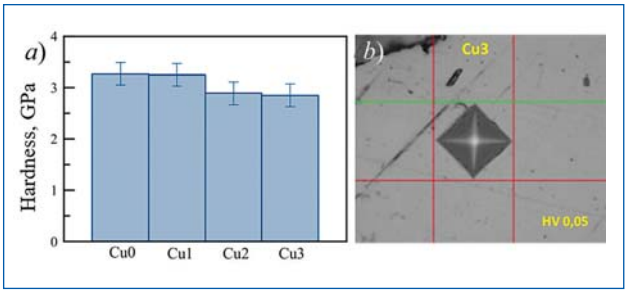

Fig. 9. Hardness of Fe–Cr–Ni–Co–Cu_x coatings (*a*), indentation zone on Cu3 coating (*b*)

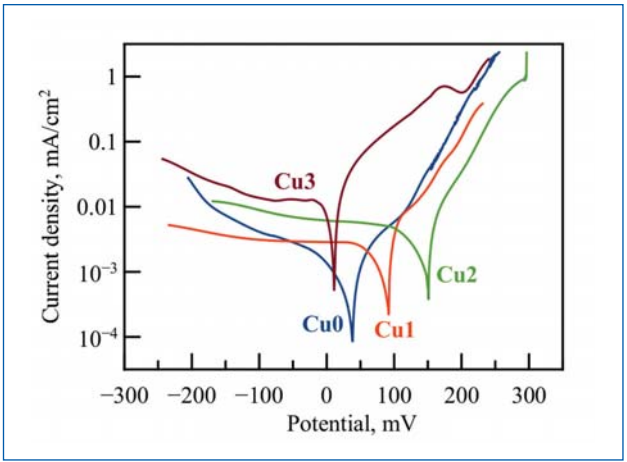

Fig. 10. Polarization curves of FeCrNiCo–Cu_x coatings

1.05 (Cu0) to 4.5 (Cu2) μA/cm². In contrary, the coating Cu3 with the maximum copper content (24 at. %) exhibited a significant drop in corrosion potential to 0 mV and the highest corrosion current density of 12 μA/cm².

It can be assumed that moderate copper alloying contributes to degradation of the passive film formed on the coating surface due to the inclusions of loose copper oxides leading to an increase in the corrosion currents. However, a more positive corrosion potential of copper leads to a monotonic shift of the coating surface potential in the positive direction. When copper concentration exceeds some threshold value (24 at. % in our case), copper accumulation on the coating surface occurs as Fe and other components dissolve. This process may result in the emergence of cathodic regions on the surface, subsequently leading to the establishment of galvanic pairs. This phenomenon initiates a pronounced increase in the corrosion current and a negative shift of the corrosion potential.

3.5. Antibacterial properties

The antibacterial properties of FeCrNiCo–Cu_x coatings were evaluated against the Gram-positive strain B. cereus Arc30, which is the dominant strain involved in biofouling. In addition, this strain is resistant to aggressive conditions.

Fig. 11 shows the CFU/mL values, after inoculation for 0, 6 and 24 h in the test solution with FeCrNiCo–Cu_x coatings. All coatings demonstrated a moderate antibacterial effect. After 6 h, Cu0 and Cu3 coatings showed 85 and 95 % decrease in CFU, respectively. Increasing the exposure time up to 24h resulted in even greater reduction of CFU up to 98.5 and 99 %. The maximum bactericidal effect (99.55 % of bacteria died) was observed for Cu2 coating. Coating Cu1 after 6h inoculation showed high antibacterial activity (98.5 CFU reduction), however, further exposure of 24h resulted in a slight increase in CFU to 97.5 %.

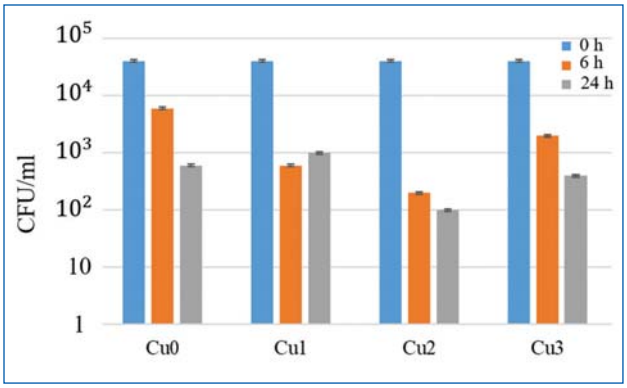

Fig. 11. Antibacterial properties of FeCrNiCo–Cu_x coatings against B. cereus Arc30

Conclusions

1) Thick (up to 23 μm) high-entropy Fe–Cr–Ni–Co–(Cu) coatings with different Cu content between 0 and 24 at. % were obtained by electrospark deposition in a protective argon atmosphere. All coatings are characterized by a single-phase structure based on solid solution with fcc lattice, dense and homogeneous microstructure with high continuity.

2) In tribocorrosion conditions, when both corrosion and wear actions are implied, coating FeCrNiCo demonstrated lowest corrosion current, while FeCrNiCo–12Cu coating revealed the most positive corrosion potential. After a certain Cu content threshold (24 at. %), tribocorrosion behavior of the FeCrNiCo–Cu_x deteriorated significantly due to formation of cathodic areas on the coating surface.

3) In terms of wear, coatings with high Cu content FeCr–NiCo–12Cu and FeCrNiCo–24Cu exhibited the highest wear resistance (6.2–6.7×10⁻⁶ mm³/Nm). Interestingly, that wear resistance did not correlate with hardness of the coatings, which is usually a case in tribocorrosion conditions.

4) All coatings demonstrated a moderate antibacterial effect against B. cereus Arc30, however, coating FeCrNiCo–12Cu was characterized by the highest ability to suppress bacterial growth and further biofilm formation.

The work was financially supported by the Russian Science Foundation (Agreement No. 20-79-10104-II).

REFERENCES

1. Tomosawa F., Tsujikawa S., Ono T., Yonemaru K., Takizawa S., Kugai Y., Minemura N. Research on Applicability of New Materials to Marine Structures in Tropical Climates: Durability Assessment of New Materials, in: *OMAE2006, Volume 3: Safety and Reliability; Materials Technology; Douglas Faulkner Symposium on Reliability and Ultimate Strength of Marine Structures*, 2006: pp. 451–460. DOI: 10.1115/OMAE2006-92110.
2. Abo Nassar N. E. Corrosion in marine and offshore steel structures: Classification and overview. *Int. J. Adv. Eng. Sci. Appl.* 2022. No. 3. pp. 7–11. DOI: 10.47346/ijaesa.v3i1.80.
3. Abbas M., Shafiee M. An overview of maintenance management strategies for corroded steel structures in extreme marine environments. *Mar. Struct.* 2020. Vol. 71. 102718. DOI: 10.1016/j.marstruc.2020.102718.
4. Alcántara J., de la Fuente D., Chico B,, Simancas J., Díaz I., Morcillo M, Marine Atmospheric Corrosion of Carbon Steel: A Review. *Materials.* 2017. No. 10. p. 406. DOI: 10.3390/ma10040406.
5. Valdez B., Ramirez J., Eliezer A., Schorr M., Ramos R., Salinas R. Corrosion assessment of infrastructure assets in coastal seas. *J. Mar. Eng. Technol.* 2016. Vol. 15. pp. 124–134. DOI: 10.1080/20464177.2016.1247635.
6. Wiener M. S., Salas B. V. Corrosion of the marine infrastructure in polluted seaports. *Corros. Eng. Sci. Technol.* 2005. Vol. 40. pp. 137–142. DOI: 10.1179/174327805X46931.
7. Xu J., Lu H., Cai L., Liao Y., Lian J. Surface Protection Technology for Metallic Materials in Marine Environments. *Materials.* 2023. Vol. 16. 6822. DOI: 10.3390/ma16206822.
8. Urbahs A., Savkovs K., Rijkuris G., Andrejeva D. Corrosion and Wear Analysis in Marine Transport Constructions. *Transp. Aerosp. Eng.* 2018. No. 6. pp. 5–14. DOI: 10.1515/tae-2018-0001.

9. Makhlouf A. S. H., Botello M. A. - Failure of the metallic structures due to microbiologically induced corrosion and the techniques for protection, Chapter 1. In: Makhlouf A. S. H., Aliofkhazraei M. (Eds.), Handb. Mater. Fail. Anal., Butterworth-Heinemann, 2018. pp. 1–18. DOI: 10.1016/B978-0-08-101928-3.00001-X.
10. Vuong P., McKinley A., Kaur P. Understanding biofouling and contaminant accretion on submerged marine structures. *Npj Mater. Degrad.* 2023. No. 7. pp. 1–11. DOI: 10.1038/s41529-023-00370-5.
11. Rajala P., Cheng D.-Q., Rice S. A. Lauro F. M. Sulfate-dependant microbially induced corrosion of mild steel in the deep sea: a 10-year microbiome study. *Microbiome*. 2022. No. 10. p. 4. DOI: 10.1186/s40168-021-01196-6.
12. Ali A., Jamil M. I., Jiang J., Shoaib M., Amin B. U., Luo S., Zhan X., Chen F., Zhang Q. An overview of controlled-biocide-release coating based on polymer resin for marine antifouling applications. *J. Polym. Res.* 2020. Vol. 27. p. 85. DOI: 10.1007/s10965-020-02054-z.
13. Dohare S. Corrosion Protection and Modern Infrastructure, in: A. Singh (Ed.), Introd. Corros., IntechOpen, Rijeka, 2023. DOI: 10.5772/intechopen.111547.
14. Larché N., Dézerville P. Review of material selection and corrosion in seawater reverse osmosis desalination plants. *Desalination Water Treat.* 2011. Vol. 31. pp. 121–133. DOI: 10.5004/dwt.2011.2362.
15. Amendola R., Acharjee A. Microbiologically Influenced Corrosion of Copper and Its Alloys in Anaerobic Aqueous Environments: A Review. *Front. Microbiol.* 2022. Vol. 13. DOI: 10.3389/fmicb.2022.806688.
16. Refait P., Grolleau A.-M., Jeannin M., Sabot R. Cathodic Protection of Complex Carbon Steel Structures in Seawater. *Corros. Mater. Degrad.* 2022. No. 3. pp. 439–453. DOI: 10.3390/cmd3030026.
17. Sun Y. Surface Engineering & Coating Technologies for Corrosion and Tribocorrosion Resistance. *Materials.* 2023. Vol. 16. p. 4863. DOI: 10.3390/ma16134863.
18. Wood R. J. K., Lu P. Coatings and Surface Modification of Alloys for Tribo-Corrosion Applications. *Coatings.* 2024. Vol. 14. p. 99. DOI: 10.3390/coatings14010099.
19. Munger C. G., Vincent L., Shifler D. A. Marine Coatings, in: LaQues Handb. Mar. Corros., John Wiley & Sons, Ltd. 2022. pp. 527–571. DOI: 10.1002/9781119788867.ch19.
20. Xavier J. R. Investigation on the effect of nano-ceria on the epoxy coatings for corrosion protection of mild steel in natural seawater. *Anti-Corros. Methods Mater.* 2018. Vol. 65. pp. 38–45. DOI: 10.1108/ACMM-04-2017-1784.
21. López-Ortega A., Bayón R., Arana J. L. Evaluation of protective coatings for offshore applications. Corrosion and tribocorrosion behavior in synthetic seawater. *Surf. Coat. Technol.* 2018. Vol. 349. pp. 1083–1097. DOI: 10.1016/j.surfcoat.2018.06.089.
22. Deng W., An Y., Zhao X., Zhang C., Tang L., Liu J. Cavitation erosion behavior of ceramic/organic coatings exposed to artificial seawater. *Surf. Coat. Technol.* 2020. Vol. 399. 126133. DOI: 10.1016/j.surfcoat.2020.126133.
23. Kumar A. M., Rajesh T., Obot I. B., Bin Sharfan I. I., Abdulhamid M. A. Water-soluble chitosan salt as ecofriendly corrosion inhibitor for N80 pipeline steel in artificial sea water: Experimental and theoretical approach. *Int. J. Biol. Macromol.* 2024. Vol. 254. 127697. DOI: 10.1016/j.ijbiomac.2023.127697.
24. Rui D., Li X., Jia W., Li W., Xiao W., Gui T. Releasing kinetics of dissolved copper and antifouling mechanism of cold sprayed copper composite coatings for submarine screen doors of ships. *J. Alloys Compd.* 2018. Vol. 763. pp. 525–537. DOI: 10.1016/j.jallcom.2018.05.355.
25. Vincent M., Hartemann P., Engels-Deutsch M. Antimicrobial applications of copper. *Int. J. Hyg. Environ. Health.* 2016. Vol. 219. pp. 585–591. DOI: 10.1016/j.ijheh.2016.06.003.
26. Rao P., Mulky L. Microbially Influenced Corrosion and its Control Measures: A Critical Review. *J. Bio- Tribo-Corros.* 2023. No. 9. p. 57. DOI: 10.1007/s40735-023-00772-7.
27. Tian J.-J., Wang K., Xu K.-W., Luo X.-T., Shao G.-S., Li C.-J. Effect of coating composition on the micro-galvanic dissolution behavior and antifouling performance of plasma-sprayed laminated-structured CuTi composite coating. *Surf. Coat. Technol.* 2021. Vol. 410. 126963. DOI: 10.1016/j.surfcoat.2021.126963.
28. Wang Z., Zhou Z., Xu W., Yang D., Xu Y., Yang L., Ren J., Li Y., Huang Y. Research status and development trends in the field of marine environment corrosion: a new perspective. *Environ. Sci. Pollut. Res.* 2021. Vol. 28. pp. 54403–54428. DOI: 10.1007/s11356-021-15974-0.
29. Javed M., Neil W., Adam G., Wade S. Microbiologically influenced corrosion of copper and its alloys–a review. *Corros. Prev.* 2016. Vol. 84. pp. 1–14.
30. Zeng Y., Yan W., Shi X., Yan M., Shan Y., Yang K. Enhanced Bio-corrosion Resistance by Cu Alloying in a Micro-alloyed Pipeline Steel. *Acta Metall. Sin. Engl. Lett.* 2022. Vol. 35. pp. 1731–1743. DOI: 10.1007/s40195-022-01392-9.
31. Jiajia Wu, Tan F., Zhang D., Yin J., Li E. Corrosion of Copper-bearing High Strength Mooring Chain Steel Affected by Microbes in Seawater. *Prot. Met. Phys. Chem. Surf.* 2019. Vol. 55. pp. 1207–1216. DOI: 10.1134/S2070205119060327.
32. Liu Z., Cui T., Chen Y., Dong Z. Effect of Cu addition to AISI 8630 steel on the resistance to microbial corrosion. *Bioelectrochemistry*. 2023. Vol. 152. 108412. DOI: 10.1016/j.bioelechem.2023.108412.
33. Li Y., Ning C. Latest research progress of marine microbiological corrosion and bio-fouling, and new approaches of marine anti-corrosion and anti-fouling. *Bioact. Mater.* 2019. No. 4. pp. 189–195. DOI: 10.1016/j.bioactmat.2019.04.003.
34. Otto F., Dlouhý A., Somsen Ch., Bei H., Eggeler G., George E. P. The influences of temperature and microstructure on the tensile properties of a CoCrFeMnNi high-entropy alloy. *Acta Mater.* 2013. Vol. 61. pp. 5743–5755. DOI: 10.1016/j.actamat.2013.06.018.
35. Guan Y., Cui X., Chen D., Su W., Zhao Y., Li J., Jin G. Realizing high strength and toughness of gradient high-entropy alloy coating by in-situ interface reaction of FeCoCrNi/FeCoCrAl. *Surf. Coat. Technol.* 2023. Vol. 464. 129569. DOI: 10.1016/j.surfcoat.2023.129569.
36. Nong Z.-S., Lei Y.-N., Zhu J.-C. Wear and oxidation resistances of AlCrFeNiTi-based high entropy alloys. *Intermetallics.* 2018. Vol. 101. pp. 144–151. DOI: 10.1016/j.intermet.2018.07.017.
37. Cheng H., Pan Z., Fu Y., Wang X., Wei Y., Luo H., Li X. Review-Corrosion-Resistant High-Entropy Alloy Coatings: A Review. *J. Electrochem. Soc.* 2021. Vol. 168. 111502. DOI: 10.1149/1945-7111/ac34d0.
38. Cui Y., Shen J., Manladan S. M., Geng K., Hu S. Wear resistance of FeCoCrNiMnAlx high-entropy alloy coatings at high temperature. *Appl. Surf. Sci.* 2020. 512. 145736. DOI: 10.1016/j.apsusc.2020.145736.
39. Duan J., Wang M., Huang R., Miao J., Lu Y., Wang T., Li T. A novel high-entropy alloy with an exceptional combination of soft magnetic properties and corrosion resistance. *Sci. China Mater.* 2023. Vol. 66. pp. 772–779. DOI: 10.1007/s40843-022-2171-5.
40. Yang W., Liu Y., Pang S., Liaw P. K., Zhang T. Bio-corrosion behavior and in vitro biocompatibility of equimolar TiZrHfNbTa high-entropy alloy. *Intermetallics.* 2020. Vol. 124. 106845. DOI: 10.1016/j.intermet.2020.106845.
41. Patel P., Roy A., Sharifi N., Stoyanov P., Chromik R. R., Moreau C. Tribological Performance of High-Entropy Coatings (HECs): A Review. *Materials.* 2022. Vol. 15. 3699. DOI: 10.3390/ma15103699.
42. Shi Y., Yang B., Liaw P. Corrosion-Resistant High-Entropy Alloys: A Review. *Metals.* 2017. No. 7. p. 43. DOI: 10.3390/met7020043.
43. Lee C. P., Chang C. C., Chen Y. Y., Yeh J. W., Shih H. C. Effect of the aluminium content of AlxCrFe1.5MnNi0.5 high-entropy alloys on the corrosion behaviour in aqueous environments. *Corros. Sci.* 2008. Vol. 50. pp. 2053–2060. DOI: 10.1016/j.corsci.2008.04.011.
44. Hsu Y.-J., Chiang W.-C., Wu J.-K. Corrosion behavior of FeCoNiCrCu$_x$ high-entropy alloys in 3.5 % sodium chloride solution. *Mater. Chem. Phys.* 2005. Vol. 92. pp. 112–117. DOI: 10.1016/j.matchemphys.2005.01.001.
45. Aliyu A., Srivastava C. Corrosion behavior and protective film constitution of AlNiCoFeCu and AlCrNiCoFeCu high entropy alloy coatings. *Surf. Interfaces.* 2021. Vol. 27. 101481. DOI: 10.1016/j.surfin.2021.101481.
46. Zheng Z. Y., Li X. C., Zhang C., Li J. C. Microstructure and corrosion behaviour of FeCoNiCuSnx high entropy alloys. *Mater. Sci. Technol.* 2015. Vol. 31. pp. 1148–1152. DOI: 10.1179/1743284714Y.0000000730.
47. Kuptsov K. A., Antonyuk M. N., Sheveyko A. N., Bondarev A. V., Ignatov S. G., Slukin P. V., Dwivedi P., Fraile A., Polcar T., Shtansky D. V., High-entropy Fe-Cr-Ni-Co-(Cu) coatings produced by vacuum electro-spark deposition for marine and coastal applications. *Surf. Coat. Technol.* 2023. Vol. 453. 129136. DOI: 10.1016/j.surfcoat.2022.129136.
48. Wang J., Wen W., Cheng J., Dai L., Li S., Zhang X., Yang Y., Li H., Hou X., Wu B., Wu J. Tribocorrosion behavior of high-entropy alloys FeCrNiCoM (M = Al, Mo) in artificial seawater. *Corros. Sci.* 2023. Vol. 218. 111165. DOI: 10.1016/j.corsci.2023.111165.
49. Wu X., Lu Y. Study on the Corrosion Resistance of Laser Clad Al0.7FeCoCrNiCux High-Entropy Alloy Coating in Marine Environment. *Coatings.* 2022. No. 12. 1855. DOI: 10.3390/coatings12121855.
50. Mukanov S., Loginov P., Fedotov A., Bychkova M., Antonyuk M., Levashov E. The Effect of Copper on the Microstructure, Wear and Corrosion Resistance of CoCrCuFeNi High-Entropy Alloys Manufactured by Powder Metallurgy. *Materials.* 2023. Vol. 16. 1178. DOI: 10.3390/ma16031178.
51. Muangtong P., Rodchanarowan A., Chaysuwan D., Chanlek N., Goodall R. The corrosion behaviour of CoCrFeNi-x (x = Cu, Al, Sn) high entropy alloy systems in chloride solution. *Corros. Sci.* 2020. Vol. 172. 108740. DOI: 10.1016/j.corsci.2020.108740.